Demonstration of Geometric Effects and Resonant Scattering in the X-Ray Spectra of High-Energy-Density Plasmas

G. Pérez-Callejo,[1,*] E. V. Marley,[2] D. A. Liedahl,[2] L. C. Jarrott,[2] G. E. Kemp,[2] R. F. Heeter,[2] J. A. Emig,[2] M. E. Foord,[2] M. B. Schneider,[2] S. J. Rose,[1,†] and J. S. Wark[1]

[1]*Department of Physics, Clarendon Laboratory, University of Oxford, Parks Road, Oxford OX1 3PU, United Kingdom*
[2]*Lawrence Livermore National Laboratory, Livermore, California 94550, USA*

(Received 24 September 2020; revised 30 November 2020; accepted 19 January 2021; published 23 February 2021)

In a plasma of sufficient size and density, photons emitted within the system have a probability of being reabsorbed and reemitted multiple times—a phenomenon known in astrophysics as resonant scattering. This effect alters the ratio of optically thick to optically thin lines, depending on the plasma geometry and viewing angle, and has significant implications for the spectra observed in a number of astrophysical scenarios, but has not previously been studied in a controlled laboratory plasma. We demonstrate the effect in the x-ray spectra emitted by cylindrical plasmas generated by high power laser irradiation, and the results confirm the geometrical interpretation of resonant scattering.

DOI: 10.1103/PhysRevLett.126.085001

Spectroscopy is a widely used method for diagnosing both astrophysical and laboratory-based high-energy-density (HED) plasmas, with a significant amount of information about the densities and temperatures of such systems being gleaned from the ratios and widths of spectral lines [1–8]. Since the earliest development of the field, it has been well known that the finite size and the geometry of the plasma should play a significant role in the observed line ratios [9], owing to the potential for multiple absorptions and re-emissions of photons from transitions with large radiative cross sections. This effect is known among the astrophysics community as resonant scattering. Such scattering plays a significant role in the analysis and characterization of the spectra of a plethora of astrophysical situations, impacting the emission from bodies as diverse as the solar corona [10–16], elliptical galaxies [17,18], and galaxy clusters [19–25]. The degree to which such so-called scattering takes place can influence estimates of the abundance of important heavy elements [26]. For example, studies of emission from the Perseus cluster have cited this phenomenon to explain the intensity of iron emission [21], although this has been disputed, and other explanations such as elemental enrichment from a supernova [22], overabundance of Ni [23], or gas movement [24] have been invoked, and thus the role of resonant scattering is still an area of active debate [27,28].

Although early on it was assumed that the main effect of resonant scattering was to scatter photons out of the line of sight [29], it was later shown that, when observing from a select range of vantage points, the geometry would exhibit itself as an enhancement in the intensity of optically thick lines over the optically thin limit [15,30–32]. Kerr *et al.* explicitly showed that this effect is related to the ratio between the line of sight (LOS) and the mean chord $\hat{l}$ of the plasma, where the LOS is defined as the length of a chord through the plasma in the direction of observation [33–35]. As photons from an optically thick line traverse the plasma, they can be reabsorbed and thus photopump the excited state of the given line, altering the upper state population from that which would be predicted in the optically thin case. If the escape path through the plasma towards the distant observer (the LOS) is smaller than $\hat{l}$, the enhancement of the emission owing to this photopumping effect is of greater importance than the attenuation due to the optical depth, while in the opposite case the emission is suppressed. Historically such optical depth effects have been introduced into the atomic kinetics modeling in a parametric manner by use of escape factors (multipliers reducing the spontaneous transition probability) [36–38] or by more sophisticated techniques which provide self-consistent solutions of both the radiative transfer equation and rate equations, as used, for example, in the Cretin code [39].

This geometric approach to resonant scattering provided a simple explanation for anomalous line ratios due to such opacity effects in certain stellar spectra [16,33], and further demonstrated that limited spatial information could be obtained merely from the spectrum, in cases where no explicit spatial resolution is possible [40] (that information being the ratio $\hat{l}$/LOS). This led to the conclusion that the O VI emission in certain solar spectra originated from a slablike geometry in the solar atmosphere rather than from cylindrical structures [41]. The same effect also plays a role in the spectra emitted from plasmas created in the laboratory, and recently a geometric analysis of dot-spectroscopy experiments at the National Ignition Facility

[42] (NIF) has yielded the first time-resolved measurements of coupled temperature and density inside an inertial confinement fusion (ICF) hohlraum [43].

Whilst there have been experimental approaches to study the effects of the geometry on the overall emitted energy in discharge [44] and certain HED plasmas [45,46], to date there has been no experimental validation of the important effect of resonant scattering in a controlled setting—i.e., within a plasma, uniform in density and temperature, and with a well-defined geometry simultaneously observed from the different relevant vantage points. It is in the above context that we report here the results from HED experiments at the OMEGA laser facility [47] at the Laboratory for Laser Energetics (LLE), in which we isolated the effect of both $\hat{l}$ and the LOS in such an experiment, and demonstrate changes in line ratios that are fully consistent with the geometric approach to resonant scattering.

In our experiments we generated two cylindrical plasmas of the same thickness and at the same conditions, with the only difference between them being their radii. This results in two plasmas with the same LOS for axial emission (face-on) but different $\hat{l}$s. Additionally, for each particular cylinder, the ratio between their axial and radial (side-on) emission provides further information about the effect of the LOS on the optically thick emission. We find how this ratio can be directly related to the size of the plasma cylinder, and in particular to its aspect ratio (thickness/radius).

The design of the experiment is based on the analysis of Kerr *et al.* [33–35] that resonant scattering can be parameterized by the ratio $f = I_{\text{thick}}/I_{\text{thin}}$, where I_{thick} is the intensity of an optically thick line, and I_{thin} is the intensity of that same line, were it and the plasma as a whole optically thin. Although this parameter f is not directly observable, one can study the ratio of emission from an optically thick line to another separate line which is optically thin, and is thus not modified by the geometry. For a given set of conditions this ratio only depends on how enhanced or suppressed the thick line is. In particular, we analyze the ratio of the resonance to the intercombination line of the Heα complex ($1s2l \rightarrow 1s^2$), hereafter referred to as w and y lines, respectively, following Gabriel's notation [48]. For mid-Z elements ($Z \sim 20$–30) under our conditions the optical depth front to back of the target of the w line at line center is ~10–20 (i.e., optically thick) whereas that of the y line is ~0.4–0.7 (optically thin).

Targets were disk-shaped foils made of a mixture of scandium and vanadium, volumetrically equal, 2000 Å thick and with two different radii, namely, 125 and 175 μm (hereafter referred to as targets R125 and R175, respectively). As shown in Fig. 1, these disks were buried in the center of a beryllium tamper, 10 μm thick and 1 mm in diameter, whose purpose was to provide a radial pressure that confines the shape of the Sc/V disks to a cylinder [49].

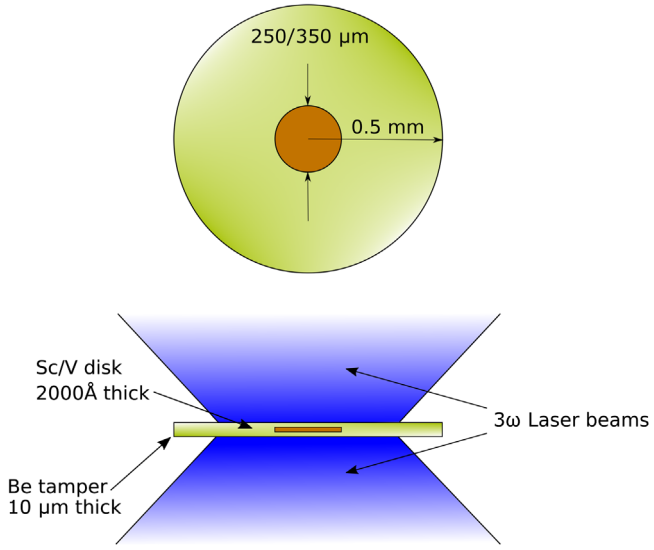

FIG. 1. Schematic drawing of the targets used in the experiment. The Sc/V disk is shown in brown whereas the Be tamper is shown in green. The thickness of the Sc/V disk has been exaggerated for clarity.

Thirty-four laser beams of 3ω light ($\lambda = 351$ nm) were shone upon the targets, 17 on each side of the tamper, using a 2.7 ns square pulse. The intensity was 3×10^{14} W cm^{-2} on each side, delivering a total energy of 10 kJ. The laser beams were focused so that the intensity was uniform across a 600 μm diameter spot, thus covering the whole extent of the Sc/V disks. The targets were observed with two multipurpose spectrometers (MSPEC) [50] and two X-ray Pinhole imaging framing cameras (XRPINH) [51]. These diagnostics were mounted such that one MSPEC and one XRPINH had a face-on view of the targets (down the axis of plasma expansion), while the other MSPEC and XRPINH had a side-on view. They were fielded sufficiently far from the target so that all rays reaching the detectors were effectively parallel, while keeping the whole target in sight. For each target radius (125 and 175 μm), we took four data shots. More details on the experimental setup are given in Ref. [46].

The irradiated embedded foils expand into cylinders of radius R, thickness H. We note that the mean chord $\hat{l}$ of convex bodies is $\hat{l} = 4V/S$ [52,53], where V and S are, respectively, the volume and surface area of the body. For a cylinder of radius R and thickness H, the LOS/$\hat{l}$ ratios for face-on and side-on view are, respectively,

$$\left.\frac{\text{LOS}}{\hat{l}}\right|_{\text{FO}} = \frac{H}{\frac{2HR}{(H+R)}} = \frac{1}{2}\left(1+\frac{H}{R}\right), \tag{1}$$

$$\left.\frac{\text{LOS}}{\hat{l}}\right|_{\text{SO}} = \frac{\frac{\pi}{2}R}{\frac{2HR}{(H+R)}} = \frac{\pi}{4}\left(1+\frac{R}{H}\right). \tag{2}$$

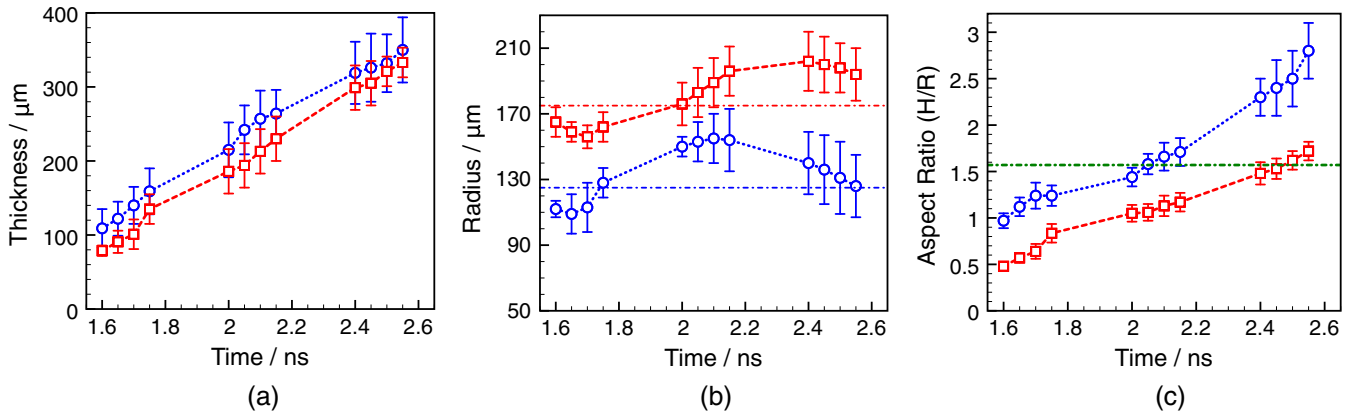

FIG. 2. Thickness H (2a), radius R (2b) and aspect ratio H/R (2c) of the R125 (blue) and R175 (red) targets as a function of time. The dot-dashed lines in both (b) indicate the initial radius of each target, while the green dot-dashed line in (c) marks an aspect ratio of $\pi/2$. The uncertainty bars correspond to shot to shot variations. Times are indicated with respect to the start of the laser pulse.

Although the escape path for face-on emission in a cylinder is always equal to the thickness H, that is not the case for the side-on emission. For that reason, in Eq. (2), we have used the mean LOS for radial view ($\pi R/2$). Note that for an aspect ratio $H/R = \pi/2$, Eqs. (1) and (2) return the same value, and that when the aspect ratio is lower than $\pi/2$, optically thick lines are enhanced in the axial direction with respect to the radial emission, while the opposite happens for aspect ratios larger than $\pi/2$.

Figure 2 shows the thickness H (2a), radius R (2b) and aspect ratio H/R (2c) of the two types of targets as a function of time, as obtained from the XRPINH images, with times indicated with respect to the start of the laser pulse. The blue circles correspond to targets R125, whereas the red squares correspond to targets R175. This color convention will be maintained for the remainder of this Letter. The additional dot-dashed lines in Fig. 2(b) indicate the initial radii of the targets. It can be seen that while both targets have the same thickness at all times, their radii are consistently different by design. This causes the aspect ratio H/R of targets R175 to be lower than that of targets R125. The green dot-dashed line in Fig. 2(c) marks a value of $\pi/2$. While for the first time steps, the aspect ratio is lower than $\pi/2$ for both types of targets, it is important to note that at 2.4 ns, the aspect ratio of targets R125 is well above the $\pi/2$ line. We denote this transition "geometric inversion."

The density of the plasma was measured from the XRPINH data, by imposing a condition of conservation of particles. The temperature distribution within the plasma was extracted by fitting the Sc and V K-shell spectra to a combination of synthetic spectra produced by the code Cretin [39] using a genetic algorithm as described in Refs. [43,54]. These are shown in Fig. 3, with the obtained temperatures on the left and the density of scandium ions on the right. For the temperature, the extent of the vertical lines corresponds to the width of the obtained temperature distribution. In the case of the densities, the error bars correspond to the uncertainty in the density from the integration time of the XRPINH. In both cases, the variation among different shots is included in the error bars. Both types of targets were found to evolve following similar temperature and density curves, therefore making it possible to directly compare their spectral emission.

A particular example of the spectral comparison is shown in Fig. 4, where the face-on emission from the Sc Heα complex for both types of targets is plotted. These spectra were taken 1.6 ns after the start of the laser pulse, and are normalised to the peak of the y line. The additional dotted lines indicate the peak of the w line and have been added to ease the comparison. It can be seen that the w line is enhanced for targets R175 with respect to targets R125. It should be noted that, although Fig. 4 serves as a visual aid, the line peaks are not direct measurements of the relative enhancement of the optically thick emission, and the line-integrated emission should be considered instead.

This is represented in Fig. 5, which shows the ratio of line-integrated face-on emission from the w to the y line for both types of targets as a function of time. These results directly show the effect of the mean chord alone in the

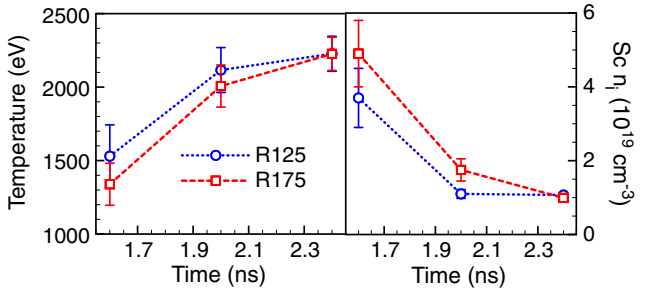

FIG. 3. Te (left) and density of scandium ions (right) for both types of targets as a function of time. Both targets evolve following the same temperature and density curves within error bars, making them comparable.

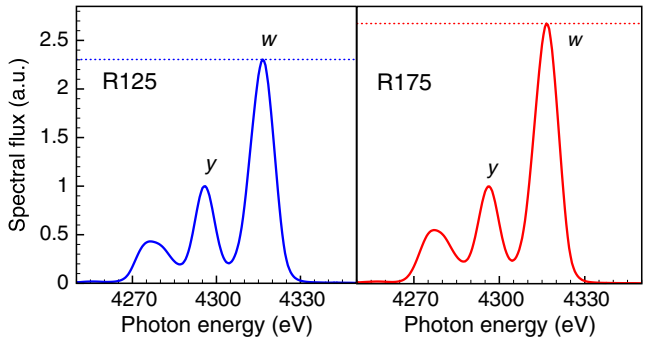

FIG. 4. Example of face-on (solid lines). The blue lines correspond to the R125 targets, while the red lines show the spectra from the R175 targets. The spectra are normalized to the peak of the y line. Additional dotted lines have been introduced in the plot to indicate the peak of the w line. These spectra were taken 1.6 ns into the laser pulse. Although both targets are at the same conditions, the w line is more enhanced with respect to the y line in the R175 targets, as their LOS is smaller with respect to the mean chord.

emission from optically thick lines. As expected, given that the aspect ratio H/R is lower for targets R175, the w line is consistently more enhanced in these targets than in targets R125, although in both cases the LOS, and temperature and density conditions are the same [as shown in Figs. 2(a) and 3]. The line ratios have been obtained following a procedure identical to that described in Ref. [46], and the error bars in the figure come from the variations in the line ratios from different shots. Additionally, the gray region shows the line ratio that corresponds to an optically thin plasma. Note that at early times, the w line is enhanced above the optically thin limit for both cases.

Alternatively, by comparing the face-on and side-on emission for a given type of target, the effect of the LOS can be studied (given that for one particular target the mean chord is unique, regardless of the direction of observation). In particular, we characterize this by using the following parameter

$$\text{Face/side} = \frac{w/y|_{\text{FO}}}{w/y|_{\text{SO}}}, \tag{3}$$

where $w/y|_{\text{view}}$ indicates the line-integrated flux ratio of the w line with respect to the y line for either face-on or side-on view. This parameter represents the relative enhancement of the w line for axial with respect to radial emission, which, to a good approximation is directly related to the ratio between both LOS's, i.e., $2H/\pi R$ [see Eqs. (1) and (2)]. Note that we are using here the mean LOS for radial emission. A more detailed treatment of the side-on emission of a plasma cylinder shows that the error introduced by this approximation is, in most cases, negligible [55].

The evolution of the face/side parameter for both types of targets is shown in Fig. 6. As the targets expand, their LOS for face-on emission (the thickness H of the cylinders) increase significantly, while for side-on emission ($\pi/2R$), the LOS stays relatively constant, as shown in Fig. 2. Therefore, the LOS for both views become more and more similar, despite the initial differences, and the relative enhancement of the optically thick lines for the face-on with respect to the side-on emission becomes less important (the face/side parameter decreases).

It is particularly interesting to note that 2.4 ns into the laser pulse, the face/side ratio of targets R125 drops below 1, while for targets R175 it does not. This is directly related to the aspect ratio of the cylinder. As shown in Fig. 2(c), at 2.4 ns, the aspect ratio of targets R125 is well above $\pi/2$ (what we referred to as geometric inversion). Therefore, the LOS for face-on view is now larger than for side-on view, which translates in the side-on emission of the optically thick w line being enhanced with

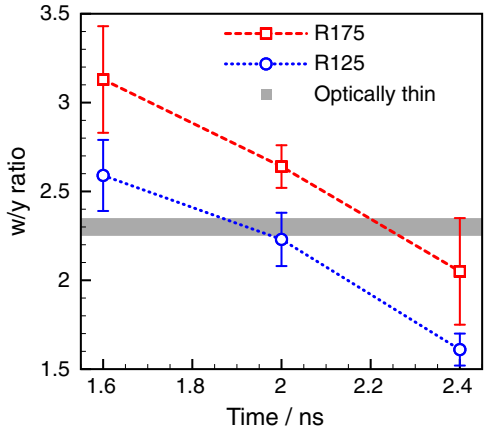

FIG. 5. Line-integrated w/y flux ratio for the face-on emission from both types of targets, and predictions for the optically thin case. Although the LOS and plasma conditions are the same in both cases, the w line is more enhanced for the R175 targets than for the R125 targets, owing to their different mean chords.

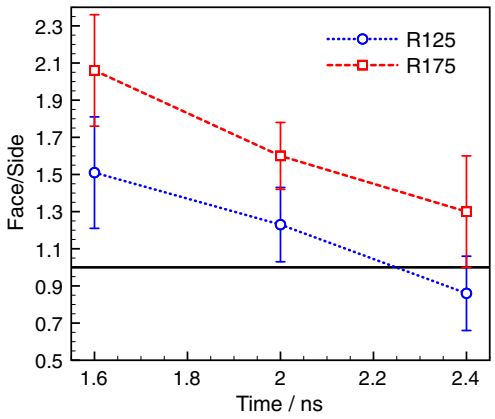

FIG. 6. Quotient between the face-on and side-on w/y ratio for both types of targets. The horizontal line corresponds to a value of 1, and defines a boundary between disklike and pipelike cylinders.

respect to its face-on emission. On the contrary, as the aspect ratio for targets R175 remains below or around $\pi/2$, this inversion does not happen, and thus the face/side ratio is greater than one. This can be understood as targets R125 becoming pipelike while targets R175 remain disklike. This is a direct measurement of changes in the geometry of the plasma obtained from the line ratios.

In conclusion, we have isolated the effects of the mean chord and the LOS on the spectra from optically thick lines in laboratory plasmas. To do so, we have created two cylindrical plasmas at the same conditions of temperature and density, with the same thicknesses, and only differing in their radii. By focusing on the axial emission from the w and y components of the Heα complex we observed significant variations on the ratio of optically thick to optically thin lines owing to the differences in the mean chord of the targets. Additionally, by comparing the face-on and side-on emission of each type of target, we have obtained the first spectroscopic observation of a geometric inversion of a plasma. These results are of direct relevance to the modeling of resonant scattering in astrophysical and ICF-related plasmas where explicit spatial resolution is impossible to obtain, and demonstrate the importance of accounting for geometry in the modelling of plasma spectra.

G. P.-C., S. J. R., and J. S. W. gratefully acknowledge support from LLNL under Grant No. B617350. This work was performed under the auspices of the U.S. Department of Energy by Lawrence Livermore National Laboratory under Contract DE-AC52-07NA27344. This document was prepared as an account of work sponsored by an agency of the United States government. Neither the United States government nor Lawrence Livermore National Security, LLC, nor any of their employees makes any warranty, expressed or implied, or assumes any legal liability or responsibility for the accuracy, completeness, or usefulness of any information, apparatus, product, or process disclosed, or represents that its use would not infringe privately owned rights. Reference herein to any specific commercial product, process, or service by trade name, trademark, manufacturer, or otherwise does not necessarily constitute or imply its endorsement, recommendation, or favoring by the United States government or Lawrence Livermore National Security, LLC. The views and opinions of authors expressed herein do not necessarily state or reflect those of the United States government or Lawrence Livermore National Security, LLC, and shall not be used for advertising or product endorsement purposes.

*gabriel.perezcallejo@physics.ox.ac.uk
†Also at Plasma Physics Group, The Blackett Laboratory, Imperial College London, Prince Consort Road, London, SW7 2AZ, United Kingdom.

[1] A. H. Gabriel and C. Jordan, Interpretation of solar helium-like ion line intensities, Mon. Not. R. Astron. Soc. **145**, 241 (1969).
[2] J. P. Apruzese, D. Duston, and J. Davis, K-shell aluminum resonance line ratios for plasma diagnosis using spot spectroscopy, J. Quant. Spectrosc. Radiat. Transfer **36**, 339 (1986).
[3] R. S. Marjoribanks, M. C. Richardson, P. A. Jaanimagi, and R. Epstein, Electron-temperature measurement in laser-produced plasmas by the ratio of isoelectronic line intensities, Phys. Rev. **46**, R1747 (1992).
[4] C. A. Back, D. H. Kalantar, R. L. Kauffman, R. W. Lee, B. K. MacGowan, D. S. Montgomery, L. V. Powers, T. D. Shepard, G. F. Stone, and L. J. Suter, Measurements of Electron Temperature by Spectroscopy in Hohlraum Targets, Phys. Rev. Lett. **77**, 4350, 1996.
[5] T. D. Shepard, C. A. Back, D. H. Kalantar, R. L. Kauffman, C. J. Keane, D. E. Klem, B. F. Lasinski, B. J. MacGowan, L. V. Powers, L. J. Suter, R. E. Turner, B. H. Failor, and W. W. Hsing, Isoelectronic x-ray spectroscopy to determine electron temperatures in lon-scale-length inertial-confinement-fusion plasmas, Phys. Rev. E **53**, R5291 (1996).
[6] J. P. Apruzese, K. G. Whitney, J. Davis, and P. C. Kepple, K-shell line ratios and powers for diagnosing cylindrical plasmas of neon, aluminum, argon, and titanium, J. Quant. Spectrosc. Radiat. Transfer **57**, 41 (1997).
[7] M. A. Barrios, D. A. Liedahl, M. B. Schneider, O. Jones, G. V. Brown, S. P. Regan, K. B. Fournier, A. S. Moore, J. S. Ross, O. Landen, R. L. Kauffman, A. Nikroo, J. Kroll, J. Jaquez, H. Huang, S. B. Hansen, D. A. Callahan, D. E. Hinkel, D. Bradley, and J. D. Moody, Electron temperature measurements inside the ablating plasma of gas-filled hohlraums at the National Ignition Facility, Phys. Plasmas **23**, 056307 (2016).
[8] M. A. Barrios *et al.*, Developing an Experimental Basis for Understanding Transport in NIF Hohlraum Plasmas, Phys. Rev. Lett. **121**, 095002 (2018).
[9] R. McWhirter, The spectroscopy of laboratory and astronomical plasmas, *Course on Plasma Diagnostics and Data Acquisition Systems, Varenna, Italy, September, 1975* (1975), A76-41027 20-75, pp. 178–244.
[10] K. Phillips, C. Greer, A. Bhatia, I. Coffey, R. Barnsley, and F. Keenan, FeXVII x-ray lines in solar coronal and laboratory plasmas, Astron. Astrophys. **324**, 381 (1997), http://adsabs.harvard.edu/pdf/1997A%26A...324..381P.
[11] J. Schmelz, J. Saba, J. Chauvin, and K. Strong, Investigating the effect of opacity in soft x-ray spectral lines emitted by solar coronal active regions, Astrophys. J. **477**, 509 (1997).
[12] J. Saba, J. Schmelz, A. Bhatia, and K. Strong, Fe XVII soft x-ray lines: Theory and data comparisons, Astrophys. J. **510**, 1064 (1999).
[13] K. Waljeski, D. Moses, K. Dere, J. Saba, K. Strong, D. Webb, and D. Zarro, The composition of a coronal active region, Astrophys. J. **429**, 909 (1994).
[14] H. Rugge and D. McKenzie, X-ray line ratios for Fe XVII observed in the solar corona, Astrophys. J. **297**, 338 (1985).
[15] K. Wood and J. Raymond, Resonant scattering of emission lines in coronal loops: Effects on image morphology and line ratios, Astrophys. J. **540**, 563 (2000).

[16] S. J. Rose, M. Matranga, M. Mathioudakis, F. P. Keenan, and J. S. Wark, Line intensity enhancements in stellar coronal x-ray spectra due to opacity effects, Astron. Astrophys. **483**, 887 (2008).
[17] T. Shigeyama, Resonance line scattering modifies x-ray surface brightness of elliptical galaxies, Astrophys. J. **497**, 587 (1998).
[18] H. Xu, S. Kahn, J. Peterson, E. Behar, F. Paerels, R. Mushotzky, J. Jernigan, A. Brinkman, and K. Makishima, High-resolution observations of the elliptical galaxy NGC 4636 with the reflection grating spectrometer on board xmm-newton, Astrophys. J. **579**, 600 (2002).
[19] R. Mitchell and R. Mushotzky, HEAO A-2 observations of the X-ray spectra of the centaurus and A1060 clusters of galaxies, Astrophys. J. **236**, 730 (1980).
[20] F. Akimoto, Y. Tawara, A. Furuzawa, A. Kumada, and K. Yamashita, Iron line mapping of cluster of galaxies and the effect of resonance scattering, *X-Ray Imaging and Spectroscopy of Cosmic Hot Plasmas, Proceedings of an International Symposium on X-ray Astronomy ASCA Third Anniversary, March*, edited by F. Makino and K. Mitsuda (Waseda University, Tokyo, 1997), p. 95.
[21] S. Molendi, G. Matt, L. Antonelli, F. Fiore, R. Fusco-Femiano, J. Kaastra, C. Maccarone, and C. Perola, How abundant is iron in the core of the Perseus cluster?, Astrophys. J. **499**, 608 (1998).
[22] R. A. Dupke and K. A. Arnaud, Central elemental abundance ratios in the Perseus cluster: Resonant scattering or sn ia enrichment?, Astrophys. J. **548**, 141 (2001).
[23] F. Gastaldello and S. Molendi, Ni abundance in the core of the Perseus cluster: An answer to the significance of resonant scattering, Astrophys. J. **600**, 670 (2004).
[24] E. Churazov, W. Forman, C. Jones, R. Sunyaev, and H. Böhringer, XMM–Newton observations of the Perseus cluster II. Evidence for gas motions in the core, Mon. Not. R. Astron. Soc. **347**, 29 (2004).
[25] E. Churazov, I. Zhuravleva, S. Sazonov, and R. Sunyaev, Resonant scattering of x-ray emission lines in the hot intergalactic medium, Space Sci. Rev. **157**, 193 (2010).
[26] M. Gilfanov, R. Syunyaev, and E. Churazov, Radial brightness profiles of resonance x-ray lines in galaxy clusters, Sov. Astron. Lett. **13**, 3 (1987), http://adsabs.harvard.edu/pdf/1987SvAL...13....3G.
[27] I. Zhuravleva, E. Churazov, R. Sunyaev, S. Sazonov, S. Allen, N. Werner, A. Simionescu, S. Konami, and T. Ohashi, Resonant scattering in the Perseus cluster: Spectral model for constraining gas motions with astro-h, Mon. Not. R. Astron. Soc. **435**, 3111 (2013).
[28] H. Collaboration, F. Aharonian, H. Akamatsu, F. Akimoto, S. W. Allen, L. Angelini, M. Audard, H. Awaki, M. Axelsson, A. Bamba *et al.*, Measurements of resonant scattering in the Perseus cluster core with Hitomi SXS, Publ. Astron. Soc. Jpn. **70**, 10 (2018).
[29] J. G. Doyle and R. W. P. McWhirter, An approximate calculation of the effect of opacity in the solar spectral lines of C III, Mon. Not. R. Astron. Soc. **193**, 947 (1980).
[30] A. K. Bhatia and S. O. Kastner, The optically thick fe xvii spectrum: X-ray, extreme-ultraviolet, and forbidden line ratios, Astrophys. J. **516**, 482 (1999).
[31] A. K. Bhatia and J. L. R. Saba, Resonance scattering of Fe XVII X-ray and extreme-ultraviolet lines, Astrophys. J. **563**, 434 (2001).
[32] S. O. Kastner and A. K. Bhatia, Optically thin and thick fe xv spectrum: Effect of self-absorption on the 284.16 resonance line, Astrophys. J. **553**, 421 (2001).
[33] F. M. Kerr, S. J. Rose, J. S. Wark, and F. P. Keenan, Enhancement of optically thick to thin line intensities in solar and stellar coronal plasmas through radiative transfer effects: An angularly resolved study, Astrophys. J. **613**, L181 (2004).
[34] F. M. Kerr, S. J. Rose, and J. S. Wark, An analytic geometry-variant approach to line ratio enhancement above the optically thin limit, Astrophys. J. **629**, 1091 (2005).
[35] F. M. Kerr, A. Gouveia, O. Renner, S. J. Rose, H. A. Scott, and J. S. Wark, Line radiation effects in laboratory and astrophysical plasmas, J. Quant. Spectrosc. Radiat. Transfer **99**, 363 (2006).
[36] T. Holstein, Imprisonment of resonance radiation in gases, Phys. Rev. **72**, 1212 (1947).
[37] T. Holstein, Imprisonment of resonance radiation in gases. II, Phys. Rev. **83**, 1159 (1951).
[38] G. J. Philips, J. S. Wark, F. M. Kerr, S. J. Rose, and R. W. Lee, Escape factors in zero-dimensional radiation-transfer codes, High Energy Density Phys. **4**, 18 (2008).
[39] H. A. Scott, CRETIN—A radiative transfer capability for laboratory plasmas, J. Quant. Spectrosc. Radiat. Transfer **71**, 689 (2001). Radiative Properties of Hot Dense Matter.
[40] P. Hatfield, Using line intensity ratios to determine the geometry of plasma in stars via their apparent areas, High Energy Density Phys. **6**, 301 (2010).
[41] F. P. Keenan, J. G. Doyle, M. S. Madjarska, S. J. Rose, L. A. Bowler, J. Britton, L. McCrink, and M. Mathioudakis, Intensity enhancement of O VI ultraviolet emission lines in solar spectra due to opacity, Astrophys. J. **784**, L39 (2014).
[42] G. H. Miller, E. I. Moses, and C. R. Wuest, The national ignition facility, Opt. Eng. **43**, 2841 (2004).
[43] G. Pérez-Callejo, M. A. Barrios, D. A. Liedahl, M. B. Schneider, O. Jones, O. Landen, R. L. Kauffman, L. J. Suter, J. D. Moody, S. J. Rose, and J. S. Wark, A novel method to measure ion density in ICF experiments using x-ray spectroscopy of cylindrical tracers, Phys. Plasmas **27**, 112714 (2020).
[44] F. Uvarov and V. Fabrikant, Experimental determination of the effective probability of photon emission by plasma atoms, Opt. Spectrosc. **18**, 323 (1965), https://ui.adsabs.harvard.edu/abs/1965OptSp..18..323U/abstract.
[45] D. M. Chambers, P. A. Pinto, J. Hawreliak, I. R. Al'Miev, A. Gouveia, P. Sondhauss, E. Wolfrum, J. S. Wark, S. H. Glenzer, R. W. Lee, P. E. Young, O. Renner, R. S. Marjoribanks, and S. Topping, K-shell spectroscopy of an independently diagnosed uniaxially expanding laser-produced aluminum plasma, Phys. Rev. E **66**, 026410 (2002).
[46] G. Pérez-Callejo, L. C. Jarrott, D. A. Liedahl, E. V. Marley, G. E. Kemp, R. F. Heeter, J. A. Emig, M. E. Foord, K. Widmann, J. Jaquez, H. Huang, S. J. Rose, J. S. Wark, and M. B. Schneider, Laboratory measurements of geometrical effects in the x-ray emission of optically thick lines for ICF diagnostics, Phys. Plasmas **26**, 063302 (2019).

[47] T. R. Boehly, D. L. Brown, R. S. Craxton, R. L. Keck, J. P. Knauer, J. H. Kelly, T. J. Kessler, S. A. Kumpan, S. J. Loucks, S. A. Letzring, F. J. Marshall, R. L. McCrory, S. F. B. Morse, W. Seka, J. M. Soures, and C. P. Verdon, Initial performance results of the OMEGA laser system, Opt. Commun. **133**, 495 (1997).

[48] A. H. Gabriel, Dielectronic satellite spectra for highly-charged helium-like ion lines, Mon. Not. R. Astron. Soc. **160**, 99 (1972).

[49] W. J. Gray, M. E. Foord, M. B. Schneider, M. A. Barrios, G. V. Brown, R. F. Heeter, L. C. Jarrott, D. A. Liedahl, E. V. Marley, C. W. Mauche, and K. Widmann, Investigation of the hydrodynamics and emission of a laser heated tamped high-z target, Phys. Plasmas **25**, 062702 (2018).

[50] R. F. Heeter, J. A. Emig, K. B. Fournier, S. B. Hansen, M. J. May, and B. K. F. Young, X-ray spectroscopy with elliptical crystals and face-on framing cameras, Rev. Sci. Instrum. **75**, 3762 (2004).

[51] F. Ze, R. Kauffman, J. Kilkenny, J. Wielwald, P. Bell, R. Hanks, J. Stewart, D. Dean, J. Bower, and R. Wallace, A new multichannel soft x-ray framing camera for fusion experiments, Rev. Sci. Instrum. **63**, 5124 (1992).

[52] P. A. M. Dirac, The Collected Works of P. A. M. Dirac 1924-1948, *Approximate Rate of Neutron Multiplication for a Solid of Arbitrary Shape and Uniform Density, I: General Theory* (Oxford University Press, New York, 1995), pp. 1115–1128.

[53] P. A. M. Dirac, K. Fuchs, R. Peierls, and P. Preston, The Collected Works of P. A. M. Dirac 1924-1948, *Approximate Rate of Neutron Multiplication for a Solid of Arbitrary Shape and Uniform Density, II: Application to the Oblate Spheroid, Hemisphere and Oblate Hemispheroid* (Oxford University Press, New York, 1995), pp. 1129–1145.

[54] E. V. Marley, D. A. Liedahl, M. B. Schneider, R. F. Heeter, L. C. Jarrott, C. W. Mauche, G. E. Kemp, M. E. Foord, Y. Frank, K. Widmann, and J. Emig, Using l-shell x-ray spectra to determine conditions of non-local thermal dynamic equilibrium plasmas, Rev. Sci. Instrum. **89**, 10F106 (2018).

[55] G. Pérez-Callejo, D. A. Liedahl, M. B. Schneider, S. J. Rose, and J. S. Wark, The use of geometric effects in diagnosing ion density in ICF-related dot spectroscopy experiments, High Energy Density Phys. **30**, 45 (2019).